Production of Λ Baryons at high Q^2 at HERA

H1 Collaboration

Abstract

The production of Λ baryons is studied using deep-inelastic events measured with the H1 detector at HERA. The measurements are made in the phase space defined by the negative four-momentum transferred squared of the photon, $145 < Q^2 < 20000\,\text{GeV}^2$, and the inelasticity $0.2 < y < 0.6$. Differential $\Lambda(\bar{\Lambda})$ production cross sections are measured. Differential $\Lambda + \bar{\Lambda}$ yields per event are determined. The $\Lambda - \bar{\Lambda}$ asymmetry is measured and found to be consistent with zero. Predictions of leading order Monte Carlo programs are compared to data.

1 Introduction

The measurement of strange particle production in high energy collisions provides valuable information for understanding Quantum Chromodynamics (QCD) in the perturbative and non-perturbative regime. The production of K_s^0, $\Lambda(\bar{\Lambda})$ has been studied at different colliders with complementary characteristics; in e^+e^- annihilation at LEP [1–4], in $p\bar{p}$ collisions at Tevatron [6], in pp interactions at RHIC [7], in ep scattering at HERA [8–13] and at the LHC [14–18].

In neutral current deep-inelastic ep scattering (DIS) at HERA the four different processes depicted in figure 1 contribute to strange hadron production. Strange quarks may be created
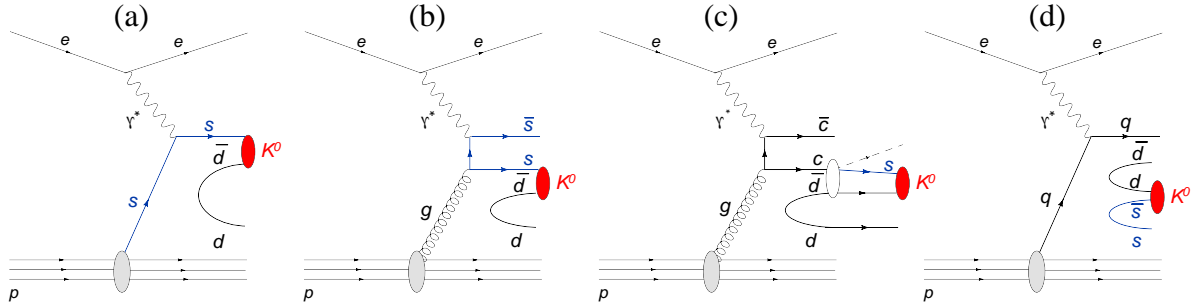

Figure 1: Schematic diagrams for the processes contributing to strangeness production in ep scattering: (a) direct production from the strange sea, (b) BGF, (c) heavy hadron decays and (d) fragmentation. The diagrams relevant for K^0 production are shown.

in the hard sub-process of the ep scattering by originating directly from the strange sea of the proton in a quark-parton-model (QPM) like interaction (figure 1a), from boson-gluon-fusion (BGF, figure 1b) or from the decays of heavy flavoured hadrons (figure 1c). In these production mechanisms hard scales are involved allowing for the applicability of perturbative QCD. The dominant source for strange hadron production, however, is the creation of an $s\bar{s}$ pairs in the non-perturbative fragmentation process (figure 1d). While strange mesons are created by all four processes strange baryon production receives only little contributions from the decays of heavy flavoured hadrons.

Since s quarks are heavy compared to u and d quarks the formation rate of $s\bar{s}$ pairs in the fragmentation process is expected to be smaller than for $u\bar{u}$ or $d\bar{d}$ pairs. Therefore the production of strange hadrons is expected to be suppressed relative to non-strange hadrons. In the modelling of the fragmentation process this suppression is generally controlled by the strangeness suppression factor λ_s. Especially, the ratio of K_s^0 to charged particles should strongly depend on this quark mass effect.

Apart from the differences in K_s^0 and Λ production observed in decays of charm and beauty hadrons the production rate of strange baryons is expected to be small relative to strange mesons as a consequence of the fragmentation process. Even if the s quark is directly produced in the hard sub-process, i.e. by the QPM or BGF process, the creation of a strange baryon is expected to be suppressed because a di-quark system from the vacuum is needed to form the baryon.

In ep scattering the initial state has a baryon quantum number of $B = 1$. The study of baryon production may therefore provide information about the process of baryon number transfer. In particular, data on the $\Lambda - \bar{\Lambda}$ production asymmetry may help understanding this mechanism.

1

This paper presents a measurement of Λ and $\bar{\Lambda}$ production in DIS at high values of the negative four momentum transferred squared, $145 < Q^2 < 20000 \, \mathrm{GeV}^2$, in the range of lepton inelasticity $0.2 < y < 0.6$. The results are based on a data sample corresponding to an integrated luminosity of $340 \, \mathrm{pb}^{-1}$ collected with the H1 detector at HERA at a centre-of-mass energy of $319 \, \mathrm{GeV}$ in the years 2004 to 2007. The analysis is performed in a different kinematic range than covered in previous H1 publications [9, 10, 13]. Results are presented for differential cross sections of Λ, then Λ yields normalized to DIS, and the $\Lambda - \bar{\Lambda}$ asymmetry. The measurements are shown as a function of various observables characterising the DIS kinematics and the strange particles production dynamics, both in the laboratory frame and in the Breit frame [19]. The results are compared with predictions obtained from leading order Monte Carlo calculations, based on matrix elements with parton shower simulation. The rôle of the parton evolution and the strangeness suppression on Λ production is investigated.

2 Monte Carlo Simulation

Deep-inelastic ep scattering is modelled using the DJANGH [20] and the RAPGAP [21] programs, which generate hard partonic processes at the Born level at leading order in α_s (e.g. $\gamma * q \rightarrow q,\ \gamma * q \rightarrow qg\ \gamma * g \rightarrow q\bar{q}$), convoluted with the parton density function (PDF) of the proton. The PDF set CTEQ6L [22] is chosen for this analysis. The factorisation and renormalisation scales a set to $\mu_f^2 = \mu_r^2 = Q^2$. Two different approaches are used for the simulation of higher order QCD effects: in RAPGAP the parton shower approach (MEPS) is implemented in which the parton emission is ordered in transverse momentum (k_T) according to the leading-log approximation; and in DJANGOH the colour dipol approach (CDM [23]) available within ARIADNE [24] is adopted in which partons are created by colour dipole radiation between the partons in the cascade, resulting in a k_T un-ordered parton emission.

The JETSET program [25] is used for simulating the hadronisation process in the Lund colour string fragmentation model [26]. The suppression of strange quarks is predominantly controlled by a single parameter, $\lambda_s = P_s/P_q$, where P_s and P_q are the probabilities for creating strange (s) or light ($q = u$ or d) quarks in the non-perturbative fragmentation process. The most relevant parameters for describing the baryon production are the di-quark suppression factor $\lambda_{qq} = P_{qq}/P_q$; i.e., the probability of producing a light di-quark pair $qq\overline{qq}$ from the vacuum with respect to a light $q\bar{q}$ pair, and the strange diquark suppression factor $\lambda_{sq} = (P_{sq}/P_{qq})/(P_s/P_q)$, which models the relative production of strange di-quark pairs. The values tuned to hadron production measurements in e^+e^--annihilation by the ALEPH collaboration [5] ($\lambda_s = 0.286$, $\lambda_{qq} = 0.108$, and $\lambda_{sq} = 0.690$) are taken herein as default values for the simulation of hadronisation within JETSET.

Monte Carlo event samples generated both with DJANGOH and RAPGAP are used for the acceptance and efficiency correction of the data. All generated events are passed through the full GEANT [27] based simulation of the H1 apparatus and are reconstructed and analysed using the same programs as for the data.

3   Experimental Procedure

3.1   The H1 Detector

A detailed description of the H1 detector can be found in [28]. In the following, only those detector components important for the present analysis are described. H1 uses a right handed Cartesian coordinate system with the origin at the nominal ep interaction point. The proton beam direction defines the positive z-axis of the laboratory frame and transverse momenta are measured in the (x, y) plane. The polar angle θ is measured with respect to this axis and the pseudorapidity η is given by $\eta = -\ln \tan \frac{\theta}{2}$.

Charged particles are measured in the Central Tracking Detector (CTD) in the range $-1.75 < \eta < 1.75$. The CTD comprises two cylindrical Central Jet Chambers (inner CJC1 and outer CJC2), arranged concentrically around the beam-line, complemented by a silicon vertex detector (CST) [29]. The CJCs are separated by a drift chamber which improves the z coordinate reconstruction. A multi-wire proportional chamber mainly used for triggering [30] is situated inside the CJC1. These detectors are arranged concentrically around the interaction region in a solenoidal magnetic field of strength 1.16 T. The trajectories of charged particles are measured with a transverse momentum resolution of $\sigma(p_T)/p_T \simeq 0.2\% \, p_T \, / \, \text{GeV} \, \oplus 0.015$. In each event the tracks are used in a common fit procedure to determine the ep interaction vertex. The measurement of the specific energy loss dE/dx of charged particles in this detector is known with a resolution of 6.3% for a minimum ionising track [31].

The tracking detectors are surrounded by a Liquid Argon calorimeter (LAr) which measures the positions and energies of particles, including that of the scattered positron, over the polar angle range $4° < \theta < 154°$. The calorimeter consists of an electromagnetic section with lead absorbers and a hadronic section with steel absorbers. The energy resolution for electrons in the electromagnetic section, as measured in beam tests, is $\sigma(E)/E = 11.5\%/\sqrt{E} \, [\, \text{GeV}\,] \oplus 1\%$ [32]. In the backward region ($153° < \theta < 178°$), particle energies are measured by a lead-scintillating fibre calorimeter (SpaCal) [33]

The DIS events studied in this paper are triggered by a compact energy deposition in the electromagnetic section of the LAr calorimeter and a signal from the multi-wire proportional chambers.

The luminosity is determined from the rate of the elastic QED Compton process $ep \rightarrow e\gamma p$, with the electron detected in the SpaCal calorimeter, and the rate of DIS events measured in the SpaCal calorimeter [34].

3.2   Selection of DIS Events

The data used in this analysis correspond to an integrated luminosity of $340 \, \text{pb}^{-1}$ and were taken by H1 in the years from 2004 to 2007 when protons with an energy of 920 GeV collided with electrons[1] with an energy of 27.6 GeV producing a centre-of-mass energy of $\sqrt{s} = 319$ GeV.

---

[1]The this paper "electron" is used to denote both electrons and positrons

DIS kinematics
$145 < Q^2 < 20000 \, \mathrm{GeV}^2$
$0.2 < y < 0.6$
Hadron kinematics
$p_T > 0.3 \, \mathrm{GeV}$
$-1.5 < \eta < 1.5$

Table 1: Analysis phase space

The selection of DIS events is based on the identification of the scattered electron as a compact calorimetric deposit in the electromagnetic section of the LAr calorimeter in the polar angular range $10° < \theta_e < 150°$, with energy greater than 11 GeV and associated with a charged track in the CTD.

At fixed centre-of-mass energies $\sqrt{s}$ the kinematics of the scattering process are described using the Lorentz invariant variables Q^2, y and x. These variables can be expressed as a function of the scattered electron energy E_e' and its scattering angle θ_e in the laboratory frame:

$$ Q^2 = 4E_e E_e' \cos^2\left(\frac{\theta_e}{2}\right), \quad y = 1 - \frac{E_e'}{E_e}\sin^2\left(\frac{\theta_e}{2}\right), \quad x = \frac{Q^2}{ys}. \tag{1} $$

The negative four-momentum transfer squared Q^2 and the inelasticity y are required to lie in the ranges $145 < Q^2 < 20000 \, \mathrm{GeV}^2$ and $0.2 < y < 0.6$. Background from photo-production events ($Q^2 \approx 0 \, \mathrm{GeV}^2$) in which the electron escapes undetected down the beam pipe and a hadron fakes the electron signature, is suppressed by the requirement that the difference $\Sigma(E - p_z)$ between the total energy and the longitudinal momentum must be in the range $35 < \Sigma(E - p_z) < 70 \, \mathrm{GeV}$, where the sum includes all measured hadronic final state particles [35] and the scattered electron candidate. The z-coordinate of the event vertex, reconstructed using the tracking detectors, has to be within ± 35 cm of the mean position for ep interactions.

3.3 Selection of Λ Baryons

The Λ baryons [2] are measured by the kinematic reconstruction of its decay $\Lambda \to p\pi^-$. The analysis is based on charged particles measured by the CTD with a minimum transverse momentum $p_T \geq 0.12 \, \mathrm{GeV}$. The Λ baryons are identified by fitting pairs of oppositely charged tracks in the (x, y) plane to their secondary decay vertices, with the direction of flight of the mother particle constrained to the primary event vertex. Candidates are required to have a minimum radial decay length of 2 cm, a minimum transverse momentum p_T of more than 300 MeV and to lie in the pseudorapidity range $|\eta| < 1.5$. The phase space of the analysis is summarised in table 1.

For the reconstruction of Λ candidates the track with the higher momentum is assumed to be the proton and the other track is assumed to be the pion. Furthermore, the observed energy loss,

---

[2]Unless otherwise noted, charge conjugate states are always implied.

dE/dx, of the proton candidates in Λ decays have to have a likelihood of being a proton of more than 0.003. The distinction between Λ and $\bar{\Lambda}$ baryon candidates is made by the electrical charge of the decay proton (antiproton) candidate. The contamination from K_s^0 decays in the Λ sample is suppressed by a rejection of the corresponding invariant mass region: $475 < M(\pi\pi) < 530$ MeV for the Λ selection. The contamination from gamma conversions is suppressed by requiring that the invariant mass, computed under the assumption that the tracks correspond to an electron–positron pair, is bigger than 50 MeV.

The number of Λ baryons is obtained by fitting the invariant mass spectra with the sum of a signal and background function. For the signal fuction a skewed t-student function is used while the background distributions are parameterised as

$$B_\Lambda(M) \;=\; p_0 \, (p_1 + p_2(M - m_\Lambda) + p_3(M - m_\Lambda)^2)(M - (m_p + m_\pi))^{p_4}. \qquad (2)$$

Here, M denotes the $p\pi$ invariant mass, and m_Λ, m_p and m_π are the nominal masses of the Λ, the proton and the pion [36]. For the differential distribution the fit is performed in each kinematic bin.

The invariant mass spectrum $M(p\pi)$ of all candidates passing the selection criteria are shown in figure 2 together with the result from the fits. In total approximately 7000 $\Lambda(\bar{\Lambda})$ baryons are reconstructed in the phase space given in table 1. The fitted Λ mass agrees with the world average [36].

4   Cross Sections Determination and Systematic Errors

The total inclusive Born-level cross section σ_{vis} in the kinematic region defined in table 1 is given by the following expression:

$$\sigma_{vis}(ep \to e\Lambda X) = \frac{N}{\mathcal{L} \cdot \epsilon \cdot BR \cdot (1 + \delta_{rad})} \qquad , \qquad (3)$$

where N represents the observed number of Λ, baryons. $\mathcal{L}$ and ϵ denote the integrated luminosity and the efficiency, respectively. The branching ratios BR for Λ decays are taken from [36]. The radiative corrections $(1 + \delta_{rad})$ needed to correct the measured cross section to the Born level are calculated using the program HERACLES [37]. The number of $\Lambda(\bar{\Lambda})$ particles is determined by fitting the mass distribution as explained in section 3.3. In the case of differential distributions the same formula is applied for each analysis bin.

The efficiency ϵ is given by $\epsilon = \epsilon_{rec} \cdot \epsilon_{trig}$, where ϵ_{rec} is the reconstruction efficiency and ϵ_{trig} is the trigger efficiency. The reconstruction efficiency includes the geometric acceptance and the efficiency for track and secondary vertex reconstruction. It is estimated using CDM Monte Carlo event samples. The trigger efficiency is extracted from the data using monitor triggers and is above 99%.

The systematic uncertainties were studied by changing in the Monte Carlo the value of the variables presented below, repeating the analysis procedure and comparing the results to the

standard analysis. For the cross section the total uncertainty was calculated adding the different contributions in quadrature, while for the ratios the uncertainties on the energy scale and angle resolution of the scattered electron, as well as on the luminosity, cancel; the other sources are assumed uncorrelated and added in quadrature. For differential distributions the systematic uncertailies are determined in each analysis bin separately. The following sources of systematic uncertainties were considered:

- the uncertainty on the energy scale of the LAr calorimeter for scattered electrons,

- the uncertainty of the measurement of the polar angle of the scattered electron,

- the uncertainty on the trigger efficiency,

- the uncertainty on the reconstruction efficiency,

- the uncertainty due the dE/dx requirement on the proton candidate,

- the uncertainty in the signal extraction due to the two different topologies, 0.2%.

- the uncertainty on the extraction of the signal,

- The uncertainty in the correction factor arising from using different Monte Carlo models in the correction procedure, taken as half of the dfference between correcting RAPGAP or DJANGO,

- the uncertainty on the branching ratio (0.5% [36]) and

- the uncertainty in the luminosity measurement.

5   Results and Discussion

5.1   Inclusive Cross Sections

The visible inclusive production cross sections σ_{vis} are measured in the kinematic region defined by $145 < Q^2 < 20000\,\mathrm{GeV}^2$ and $0.2 < y < 0.6$ for the event kinematics; and for the kinematics of the neutral strange hadrons, $p_T(\Lambda(\bar{\Lambda})) > 300\,\mathrm{MeV}$, $|\eta(\Lambda(\bar{\Lambda}))| < 1.5$. The cross sections are measured to be:

$$
\begin{aligned}
\sigma_{vis}(ep \to e[\Lambda + \bar{\Lambda}]X) &= 144.7 \pm 4.7(\text{stat.})^{+9.4}_{-8.5}(\text{syst.})\ \text{pb}, \\
\sigma_{vis}(ep \to e\Lambda X) &= 72.6 \pm 3.3(\text{stat.})^{+4.8}_{-4.5}(\text{syst.})\ \text{pb}, \\
\sigma_{vis}(ep \to e\bar{\Lambda} X) &= 72.9 \pm 4.0(\text{stat.})^{+4.9}_{-4.6}(\text{syst.})\ \text{pb}
\end{aligned}
$$

The cross section predictions for $\Lambda + \bar{\Lambda}$ production from the MEPS and CDM models are shown in Table 2 for two values of the strangeness suppression parameter λ_s . The measured inclusive $\Lambda + \bar{\Lambda}$ cross section is close to the CDM prediction with $\lambda_s = 0.22$ and to the MEPS prediction with $\lambda_s = 0.286$.

6

	$\lambda_s = 0.220$	$\lambda_s = 0.286$
$\sigma_{vis}(ep \rightarrow e[\Lambda + \bar{\Lambda}]X)$ CDM	136 pb	161 pb
$\sigma_{vis}(ep \rightarrow e[\Lambda + \bar{\Lambda}]X)$ MEPS	120 pb	144 pb

Table 2: Monte Carlo predictions for different settings of the strangeness suppresion factor λ_s.

5.2 Differential cross sections

Differential $\Lambda + \bar{\Lambda}$ cross sections are presented as a function of the kinematics of DIS and of the strange particles, both in the laboratory and in the Breit frame of references. The results in the Breit frame are presented separately for the current and target hemispheres.

The measurement of the differential cross section as a function of the kinematic variables of DIS, Q^2 and x, as well as the kinematic variables of the neutral strange hadrons in the laboratory frame, p_T and η, are shown in Figure 3 along with the predictions of the MEPS and CDM models for λ_s values of 0.220 and 0.286. The cross sections fall rapidly as Q^2, x and p_T grow. The models follow the general behaviour of data, but some differences are seen.

In the Breit frame of reference the virtual space-like moment transferred in the interaction has no energy. The direction of q_μ, where $Q^2 = -q_\mu q^\mu$, defines the negative z-axis, with the proton moving in the positive z direction. The transverse momentum in the Breit frame is computed with respect to this axis. Particles with a positive z component of their momenta, as expected from those particles produced close to the proton remnant, are assigned to the target hemisphere; while those having negative z component of their momenta, as expected for particles close to the direction of the struck quark in the naive quark-parton model, are assigned to the current hemisphere. In the figures these hemispheres are denoted by BFT and BFC, respectively.

It is expected that the production of particles in the current hemisphere resembles that of e^+e^- collisions. In analogy with the fragmentation variable use in those cases, for ep collisions it is customary to define $x^{\mathrm{BF}} = 2|p^{BF}|/Q$ where p^{BF} is the three momentum of the strange particle in the Breit frame. The variables x^{BFT} and x^{BFC} are obvious generalisations to take into account if the particle is assigned to the target or current hemisphere respectively.

The measured differential $\Lambda + \bar{\Lambda}$ production cross sections in the Breit frame are shown in Figure 4. The cross sections fall rapidly in all cases. They are bigger in the current than in the target hemisphere, which is opposite to the behaviour observed at lower values of Q^2 [13]. This is expected due the kinematical effects at high Q^2 which push the target region more forward while the current region starts to fill the CJC.

5.3 Λ Production to DIS Cross Section Ratio

By normalising the particle production cross section to the DIS cross section many model dependent uncertainties, like the cross section dependence on proton PDFs, cancel thus enhancing

7

the sensitivity on details of the fragmentation process. In Figure 5 the ratio of Λ production to DIS cross section is shown as a function of Q^2, and x in comparison to the expectations from RAPGAP and DJANGOH both using $\lambda_s = 0.286$ and $\lambda_s = 0.220$. The DJANGOH prediction with $\lambda_s = 0.286$ yields the worst description of the data by overshoots them significantly independent of Q^2 and x. For the same strangeness suppression factor also RAPGAP tends to yield ratios larger than observed in data for $Q^2 < 200\,\text{GeV}^2$. The best description is provided by DJANGHO using $\lambda_s = 0.220$.

5.4 Λ– $\bar{\Lambda}$ Asymmetries

The Λ– $\bar{\Lambda}$ asymmetry is defined as:

$$A_\Lambda = \frac{\sigma_{vis}(ep \to e\Lambda X) - \sigma_{vis}(ep \to e\bar{\Lambda}X)}{\sigma_{vis}(ep \to e\Lambda X) + \sigma_{vis}(ep \to e\bar{\Lambda}X)}. \tag{4}$$

This observable could shed light on the mechanism of baryon number transfer in ep scattering. A significant positive asymmetry would be an indication for the baryon number transfer from the proton to the Λ baryon. If present such an effect should be more pronounced in the positive η region in the laboratory frame and in the target hemisphere in the Breit frame. For the kinemaic region defined in table 1 the asymmetry is measured to be

$$A_\Lambda = 0.002 \pm 0.022\,(\text{stat.}) \pm 0.018\,(\text{syst.}).$$

In figure 6 and 7 A_Λ is shown as a function of the variables measured in the laboratory frame and the Breit frame, respectively. Also when studying the asymmetry as a function of these variables the data data do not show any evidence for a non-vanishing asymmetry in the phase space region investigated.

6 Conclusions

This paper presents a study of inclusive Λ production in DIS at high Q^2 measured with the H1 detector at HERA. The kinematic range of the analysis covers the phase space region $145 < Q^2 < 20000\,\text{GeV}^2$, and $0.2 < y < 0.6$. The Λ production cross section are measured as a function of the DIS variables Q^2 and x and of Λ production variables in the laboratory and in the Breit frames of reference. The measurements in the Breit frame are presented separately for the target and current hemispheres. In addition results on the Λ production to DIS cross section ratio and the $\Lambda - \bar{\Lambda}$ asymmetry are presented.

The measurements are been compared to model predictions of DJANGOH, based on the colour-dipol model (CDM)and RAPGAP based on DGLAP matrix element calculations supplemented parton showers (MEPS). Two different values of the strangeness suppression factor λ_s (0.220 and 0.286) are used for both models. The measured visible Λ cross section is found to be described best by the CDM using $\lambda_s = 0.220$ and the MEPS model using $\lambda_s = 0.286$. When investigating the Λ production to DIS cross section ratio the best agreement is observed for the CDM with $\lambda_s = 0.220$. The $\Lambda - \bar{\Lambda}$ asymmetry is found to be consistent with zero.

References

[1] D. Buskulic *et al.* [ALEPH Collaboration], "Production of K0 and Lambda in hadronic Z decays," Z. Phys. **C64**, 361-374 (1994).

[2] M. Acciarri *et al.* [L3 Collaboration], "Measurement of inclusive production of neutral hadrons from Z decays," Phys. Lett. **B328**, 223-233 (1994).

[3] P. Abreu *et al.* [DELPHI Collaboration], "Production characteristics of K0 and light meson resonances in hadronic decays of the Z0," Z. Phys. **C65**, 587-602 (1995).

[4] P. D. Acton *et al.* [OPAL Collaboration], "A Measurement of strange baryon production in hadronic Z0 decays," Phys. Lett. **B291**, 503-518 (1992).

[5] R. Barate *et al.* [ALEPH Collaboration], "Studies of quantum chromodynamics with the ALEPH detector," Phys. Rept. **294** (1998) 1.

[6] D. Acosta *et al.* [CDF Collaboration], "K_S^0 and Λ^0 production studies in $p\bar{p}$ collisions at $\sqrt{s} = 1800$-GeV and 630-GeV," Phys. Rev. **D72**, 052001 (2005). [hep-ex/0504048].

[7] B. I. Abelev *et al.* [STAR Collaboration], "Strange particle production in p+p collisions at s**(1/2) = 200-GeV," Phys. Rev. **C75**, 064901 (2007). [nucl-ex/0607033].

[8] M. Derrick *et al.* [ZEUS Collaboration], "Neutral strange particle production in deep inelastic scattering at HERA," Z. Phys. **C68**, 29-42 (1995). [hep-ex/9505011].

[9] S. Aid *et al.* [H1 Collaboration], "Strangeness production in deep inelastic positron - proton scattering at HERA," Nucl. Phys. **B480**, 3-34 (1996). [hep-ex/9607010].

[10] C. Adloff *et al.* [H1 Collaboration], "Photoproduction of K0 and Lambda at HERA and a comparison with deep inelastic scattering," Z. Phys. **C76**, 213-221 (1997). [hep-ex/9705018].

[11] J. Breitweg *et al.* [ZEUS Collaboration], "Charged particles and neutral kaons in photo-produced jets at HERA," Eur. Phys. J. **C2**, 77-93 (1998). [hep-ex/9711018].

[12] S. Chekanov *et al.* [ZEUS Collaboration], "Measurement of K_S^0, Λ, $\bar{\Lambda}$ production at HERA," Eur. Phys. J. **C51**, 1-23 (2007). [hep-ex/0612023].

[13] F. D. Aaron *et al.* [H1 Collaboration], "Strangeness Production at low Q**2 in Deep-Inelastic ep Scattering at HERA," Eur. Phys. J. **C61**, 185-205 (2009). [arXiv:0810.4036 [hep-ex]].

[14] K. Aamodt, A. Abrahantes Quintana, D. Adamova, A. M. Adare, M. M. Aggarwal, G. Aglieri Rinella, A. G. Agocs, S. Aguilar Salazar *et al.*, "Strange particle production in proton-proton collisions at sqrt(s) = 0.9 TeV with ALICE at the LHC," Eur. Phys. J. **C71**, 1594 (2011). [arXiv:1012.3257 [hep-ex]].

[15] V. Khachatryan *et al.* [CMS Collaboration], "Strange Particle Production in pp Collisions at sqrt(s) = 0.9 and 7 TeV," JHEP **1105**, 064 (2011). [arXiv:1102.4282 [hep-ex]].

[16] RAaij *et al.* [LHCb Collaboration], "Prompt Kshort production in pp collisions at sqrt(s)=0.9 TeV," Phys. Lett. **B693**, 69-80 (2010). [arXiv:1008.3105 [hep-ex]].

[17] R. Aaij *et al.* [LHCb Collaboration], "Measurement of V^0 production ratios in pp collisions at $\sqrt{s} = 0.9$ and 7 TeV," JHEP **1108**, 034 (2011). [arXiv:1107.0882 [hep-ex]].

[18] G. Aad *et al.* [ATLAS Collaboration], Phys. Rev. **D 85** (2012) 012001 [arXiv:1111.1297].

[19] R. P. Feynman, "Photon-Hadron-Interactions", Benjamin, New York (1972).

[20] G. A. Schuler and H. Siesberger, DJANGO, Proceedings of "Physics at HERA", eds. W. Buchmüller and G. Ingelman, DESY, Hamburg (1992) 1419.

[21] H. Jung, "Hard diffractive scattering in high-energy e p collisions and the Monte Carlo generator RAPGAP," Comp. Phys. Commun. 86 (1995) 147.

[22] J. Pumplin *et al.*, JHEP **0207** (2002) 012, [hep-ph/0201195].

[23] B. Andersson *et al.* "Coherence Effects in Deep Inelastic Scattering," Z. Phys. C **43** (1989) 625;
L. Lönnblad, "Rapidity gaps and other final state properties in the colour dipole model for deep inelastic scattering," Z. Phys. C **65** (1995) 285.

[24] L. Lönnblad, "Ariadne Version 4: A Program For Simulation Of QCD Cascades Implementing The Colour Dipole Model," Ariadne version 4, Comput. Phys. Commun. **71** (1992) 15.

[25] T. Sjöstrand, "High-energy physics event generation with PYTHIA 5.7 and JETSET 7.4," Comput. Phys. Commun. **82** (1994) 74, JETSET version 7.4 is used.

[26] T. Sjöstrand, "The Lund Monte Carlo For Jet Fragmentation And E+ E- Physics: Jetset Version 6.2," Comput. Phys. Commun. **39** (1986) 347;
T. Sjöstrand and M. Bengtsson, "The Lund Monte Carlo For Jet Fragmentation And E+ E- Physics. Jetset Version 6.3: An Update," Comput. Phys. Commun. **43** (1987) 367;
B. Andersson *et al.* "Parton Fragmentation And String Dynamics," Phys. Rept. **97** (1983) 31.

[27] R. Brun *et al.* GEANT3, Technical Report CERN-DD/EE/84-1, CERN, 1987.

[28] I. Abt *et al.* [H1 Collaboration], "The H1 detector at HERA," Nucl. Instrum. Meth. A **386** (1997) 310;
I. Abt *et al.* [H1 Collaboration], "The Tracking, calorimeter and muon detectors of the H1 experiment at HERA," Nucl. Instrum. Meth. A **386** (1997) 348.

[29] D. Pitzl *et al.*, "The H1 silicon vertex detector," Nucl. Instrum. Meth. A **454** (2000) 334 [hep-ex/0002044].

[30] J. Becker *et al.*, "A Vertex Trigger based on Cylindrical Multiwire Proportional Chambers" Nucl. Instrum. Meth. A **586** (2008) 190, [physics/0701002].

[31] E. Hennekemper, "Simulation and Calibration of the Specific Energy Loss of the Central Jet Chambers of the H1 Detector and Measurement of the Inclusive D^* Meson Cross Section in Photoproduction at HERA", Ph.D. thesis, Univ. Heidelberg (2011), HD-KIP-11-68 (available at http://www-h1.desy.de/publications/thesis_list.html).

[32] B. Andrieu *et al.* [H1 Calorimeter Group], "Beam tests and calibration of the H1 liquid argon calorimeter with electrons," Nucl. Instrum. Meth. A **350** (1994) 57.

[33] R.D. Appuhn *et al.*, "The H1 lead/scintillating-fibre calorimeter," Nucl. Instrum. Meth. A **386** (1997) 397.

[34] F.D. Aaron *et al.* [H1 Collaboration], "Determination of the Integrated Luminosity at HERA using Elastic QED Compton Events", Eur. Phys J. **C72** (2012) 2163, [arXiv:1205.2448].

[35] M. Peez, 'Recherche de déviations au Modèle Standard dans les processus de grande énergie transverse sur le collisionneur électron-proton HERA', PhD thesis (in French), Université de Lyon (2003), DESY-THESIS-2003-023
available at http://www-h1.desy.de/publications/theses_list.html;
S. Hellwig, 'Untersuchung der D^*-π_{slow} Double Tagging Methode in Charmanalysen', Dipl. thesis (in German), Univ. Hamburg (2004)
available at http://www-h1.desy.de/publications/theses_list.html.

[36] K. Nakamura et al. (Particle Data Group), J. Phys. G 37, 075021 (2010).

[37] A. Kwiatkowski, H. Spiesberger and H. J. Möhring, "HERACLES: An Event Generator for e p Interactionsat HERA Energies including Radiative Processes: Version 1.0," HERACLES version 1.0, Comput. Phys. Commun. **69** (1992) 155.
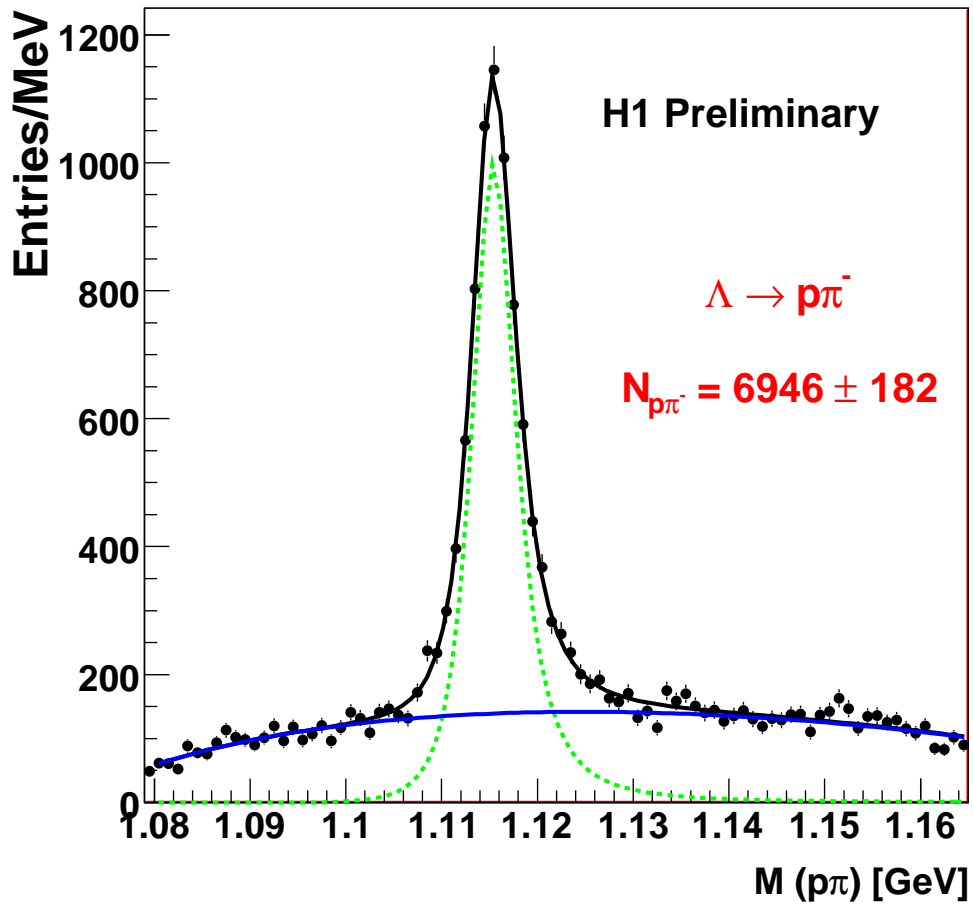
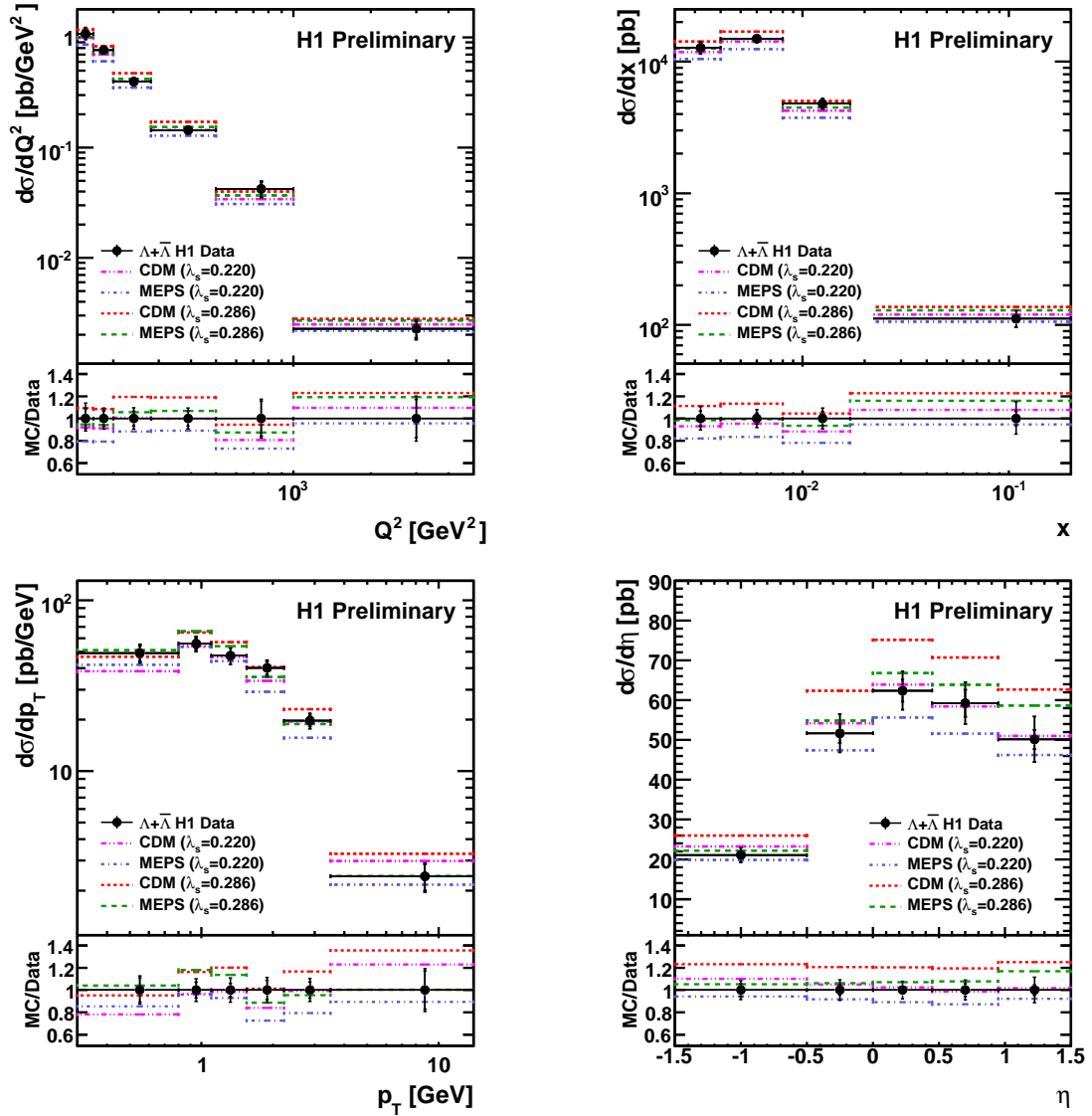Figure 2: Mass distributions for $\Lambda + \bar{\Lambda}$ candidates.

Figure 3: Differential $\Lambda + \bar{\Lambda}$ production cross sections as a function of (a) the photon virtuality squared Q^2, (b) Bjorken scaling variable x, (c) the transverse momentum, p_T, of the Λ baryon and (d) its pseudorapidity η in comparison to RAPGAP (MEPS) and DJANGOH (CDM) with two different vaues of λ_s. The inner (outer) error bars show the statistical (total) errors. The "MC/Data" ratios are shown for different Monte Carlo predictions. For comparison, the data points are put to one.
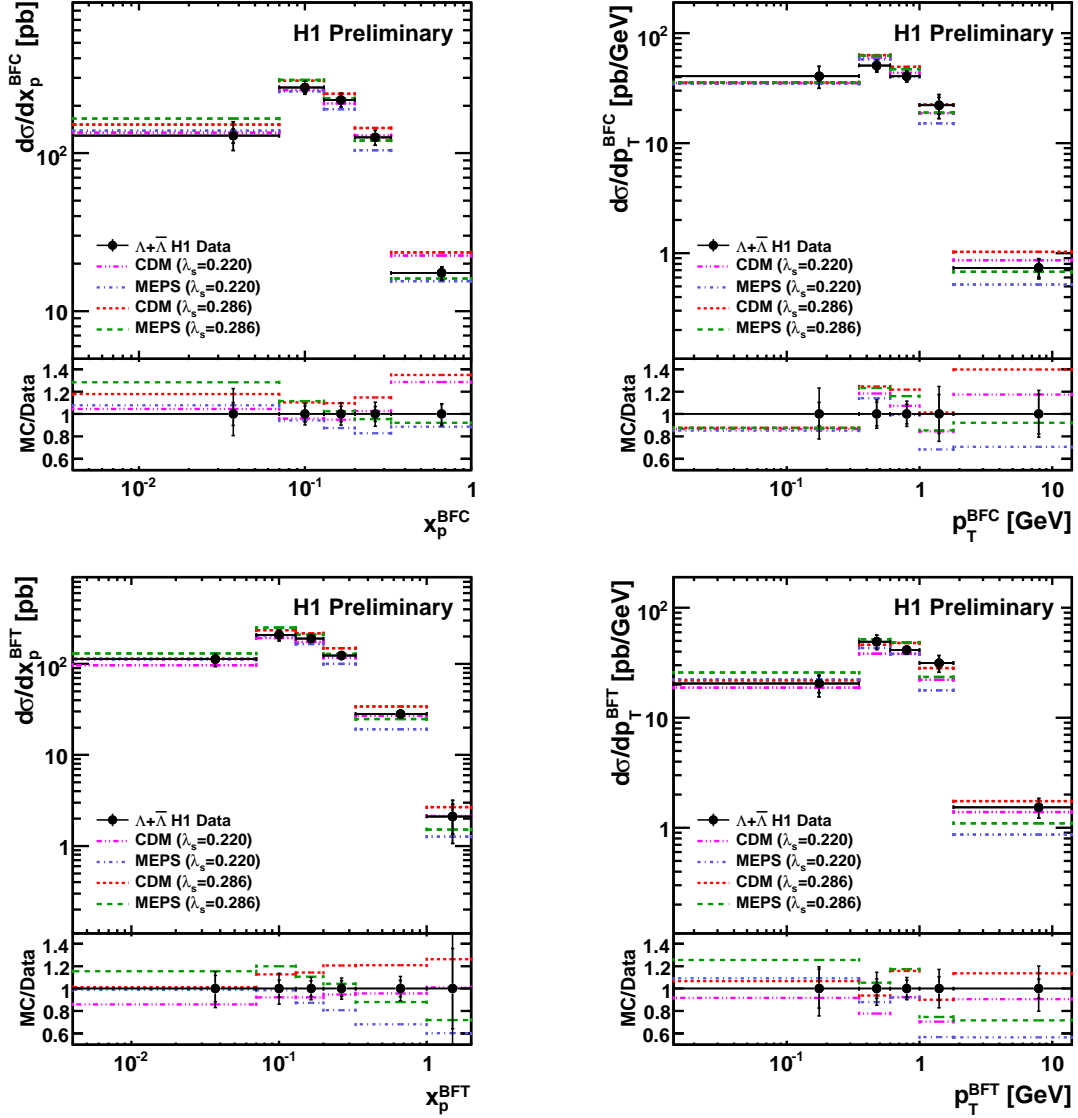
Figure 4: Differential Λ production cross sections in the Breit frame as a function of (a) p_T^{BFC}, (b) x^{BFC}, (c) p_T^{BFT}, (d) x^{BFT} in comparison to RAPGAP (MEPS) and DJANGOH (CDM) with two different vaues of λ_s. The inner (outer) error bars show the statistical (total) errors. The "MC/Data" ratios are shown for different Monte Carlo predictions. For the ratios the data points are put at one for comparison.
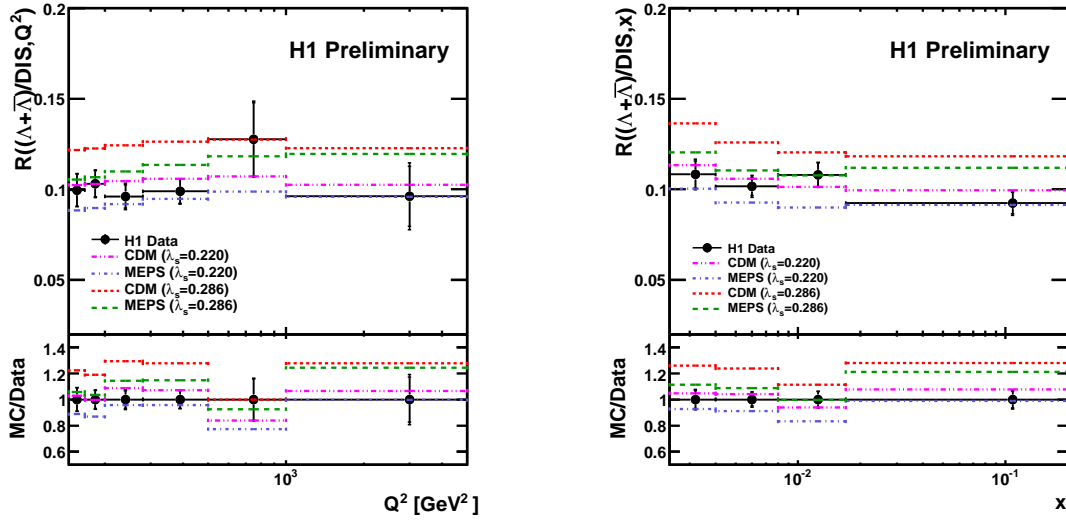
14

Figure 5: Ratio R(DIS) of Λ production to DIS cross section as a function of (a) the photon virtuality squared Q^2 and (b) Bjorken scaling variable x in comparison to RAPGAP (MEPS) and DJANGOH (CDM) with two different vaues of λ_s. The inner (outer) error bars show the statistical (total) errors. The "MC/Data" ratios are shown for different Monte Carlo predictions. For the ratios the data points are put at one for comparison.
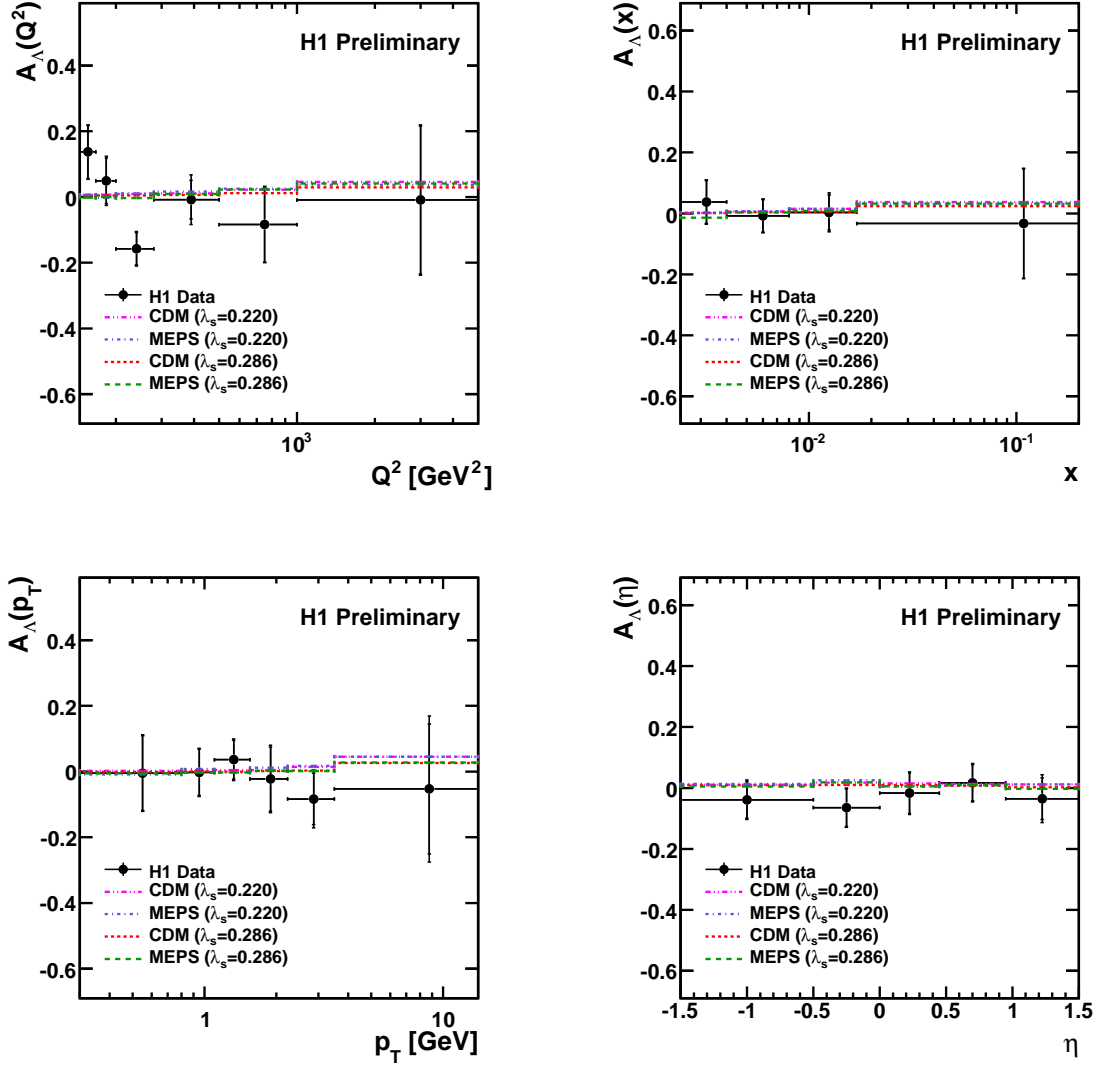
15

Figure 6: Asymmetry A_Λ as a function of (a) the photon virtuality squared Q^2, (b) Bjorken scaling variable x, (c) the transverse momentum, p_T and (d) its pseudorapidity η in the laboratory frame in comparison to RAPGAP (MEPS) and DJANGOH (CDM) with two different vaues of λ_s.
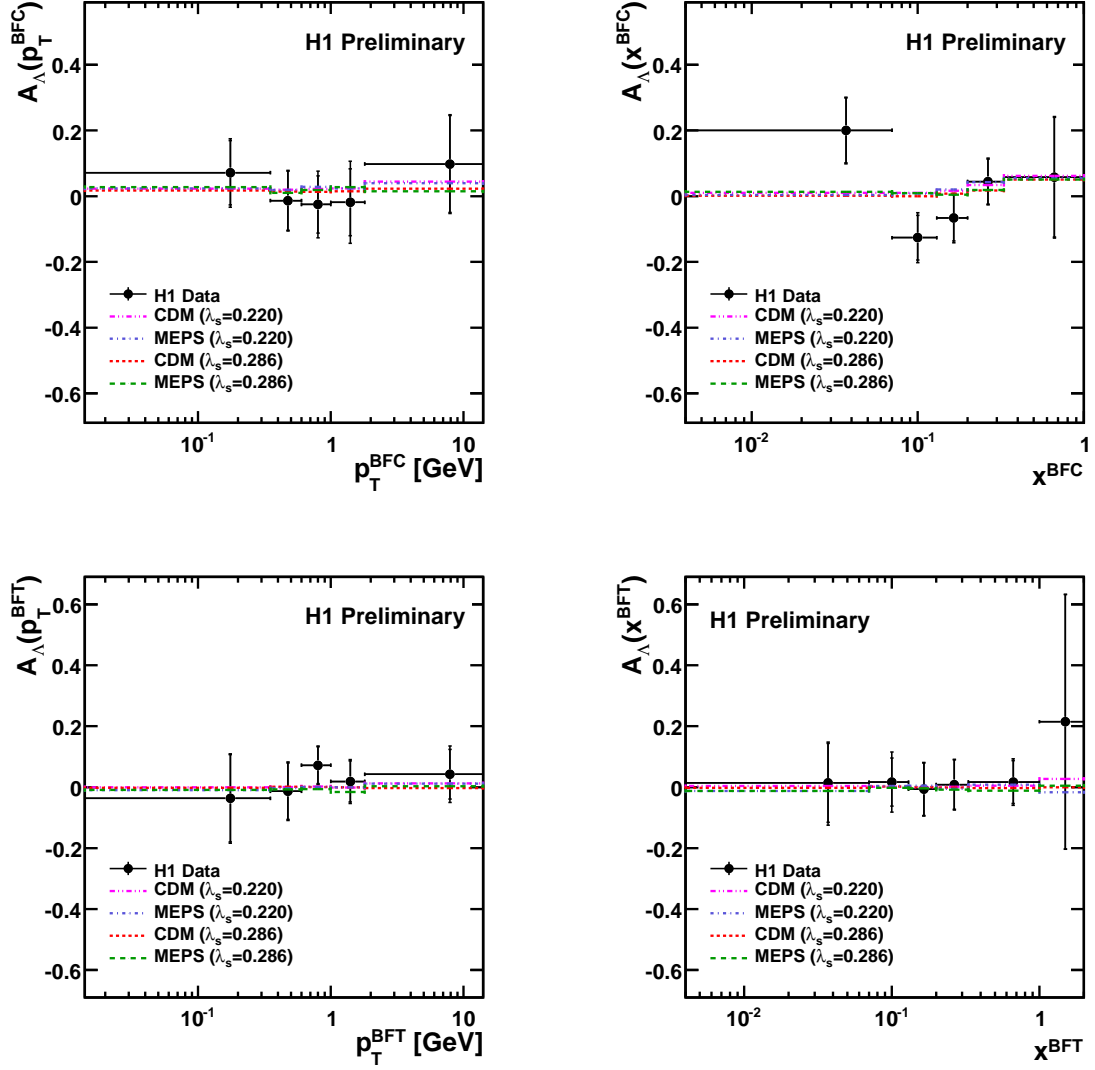
Figure 7: Asymmetry A_Λ as a function of the Breit frame variables (a) p_T^{BFC}, (b) x^{BFC}, (c) p_T^{BFT}, (d) x^{BFT} in comparison to RAPGAP (MEPS) and DJANGOH (CDM) with two different vaues of λ_s.